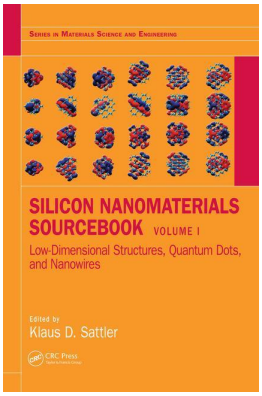

Silicon Nanomaterials Sourcebook
Low-Dimensional Structures Nanopowders, Nanowires

Klaus D. Sattler

Fluorescent silicon clusters and nanoparticles

Publication details
https://test.routledgehandbooks.com/doi/10.4324/9781315153544-10
Klaus von Haeften
Published online on: 09 Aug 2017

8 Fluorescent silicon clusters and nanoparticles

Klaus von Haeften

Contents

8.1 INTRODUCTION

Clusters, consisting of a small number of atoms, have been in the focus of physical and chemical research for several decades. They often show dramatic size effects. The addition of a single atoms can change their properties rather abruptly because of, for example, the discreteness of shell filling (Knight et al. 1984) or sphere-packing effects (Echt et al. 1981). When clusters become larger and reach the nanometer scale, other effects are observed, such as quantum confinement; the intense red fluorescence observed for nanostructured silicon (Canham 1990; Cullis and Canham 1991; Wilson et al. 1993; Lockwood 1994; Cullis et al. 1997) is a popular and frequently cited example of this effect. The discovery of fluorescent nanoscale silicon at room temperature by Canham (Canham 1990) increased the already quite intense research into silicon clusters further, and to date numerous examples of nanostructured forms of fluorescent silicon have been reported (Takagi et al. 1990; Brus et al. 1995; Hirschman et al. 1996; Borsella et al. 1997; Ehbrecht et al. 1997; Cullis et al. 1997; Huisken et al. 1999; Pavesi et al. 2000; Belomoin et al. 2000, 2002; Falconieri et al. 2005; Mangolini et al. 2005; Brewer and von Haeften 2009; Vincent et al. 2010; He et al. 2011; Dasog et al. 2014; Li et al. 2016). Hence, we have a rich set of data available on electronic and structural properties that underpin our understanding of the fluorescence of silicon clusters and nanoparticles.

The strong appeal of fluorescent silicon clusters and nanoparticles arises due to a veritable multitude of applications, for example, in electronic circuits (Pavesi 2003; Švrček et al. 2004; Stupca et al. 2007) and biomedicine (Nel et al. 2009; Chinnathambi et al. 2014). Silicon is the most frequently used semiconductor material in electronics. It has been suggested that by combining electric and optical signal transmission, higher performance can be achieved (Canham 2000; Pavesi 2003). Issues directly related to the decreasing size of electronic units, such as signal delay caused by increasingly longer interconnects, can be addressed by optically transmitted refresh pulses (Pavesi 2003). Fluorescent silicon clusters and nanoparticles are also attractive in biomedical applications because nanoscale silicon and silicon dioxide are considered to be nontoxic, or at least considerably less harmful than fluorescent nanoparticles of other materials (Warner et al. 2005; Erogbogbo and Swihart 2007; Erogbogbo et al. 2008; Choi et al. 2009;

Erogbogbo et al. 2010; Cheng et al. 2014; McVey and Tilley 2014; Peng et al. 2014) as well as biodegradable (Park et al. 2009). Fluorescent silicon nanoparticles play an important role as biological markers (Nel et al. 2009; Montalti et al. 2015).

In this chapter, the foundations of silicon cluster experiments and cluster production will be discussed. The underlying principles behind the fluorescence of silicon clusters and nanoparticles, such as quantum confinement and surface passivation, are introduced, and contrasted with the current state of research on fluorescent silicon clusters and nanoparticles. Owing to the vast number of publications on this subject that can already be found in the literature, this book chapter cannot be exhaustive. Rather, it complements recent review articles on fluorescent nanoscale silicon (Cheng et al. 2014; Dohnalová et al. 2014; McVey and Tilley 2014; Peng et al. 2014; Priolo et al. 2014; Montalti et al. 2015; Dasog et al. 2016).

8.2 FUNDAMENTAL CONCEPTS FOR PRODUCING FLUORESCENT NANOSCALE SILICON

Bulk crystalline silicon is known as a poor light emitter because of its indirect band gap. Fluorescence is a relatively inefficient relaxation process in electronically excited indirect band gap semiconductors because fluorescence has to simultaneously occur with the absorption of a phonon of matching momentum. This mechanism is illustrated in more detail in Figure 8.1. The entire electronic excitation and relaxation/fluorescence cycle is shown for direct and indirect band gap semiconductors.

The left-hand side of Figure 8.1 shows an energy band schematic of a direct band gap semiconductor, characterized by the conduction and valence band maxima and minima being on top of each other. Photoexcitation of an electron follows an energetic pathway indicated by the vertical arrow, reaching from the top of the valence band and into the conduction band, from where it returns to recombine with the hole, inducing fluorescence. Photoexcitation using higher energies is possible, but less likely because of the decreasing density of states along the parabola, and indeed the fluorescence wavelength will remain unaltered because of the relatively short timescale on which electronic relaxation occurs in the conduction and valence bands. The fluorescence intensity will be unchanged because both electron and hole have the same momentum.

This situation changes in indirect band gap semiconductors, as shown on the right-hand side in Figure 8.1. In indirect band gap semiconductors, the minima of the conduction band and maxima of the valence band are shifted. As a consequence, electrons that are photoexcited into the conduction bands quickly undergo electronic relaxation to the minimum of the conduction band. However, any subsequent direct, vertical decay to the valence band is not possible because all states with similar momenta, $\hbar k$, are populated with electrons; in other words, hole states for direct recombination with the excited electrons are not available. "Diagonal" recombination with the available, original hole state at the maximum of the

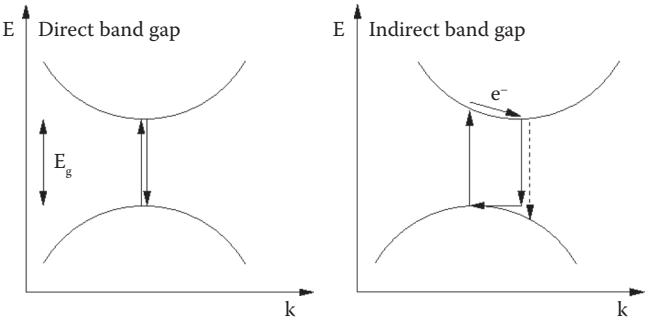

Figure 8.1 Schematic of fluorescence emission in direct and indirect band gap semiconductors. The scheme shows the valence (bottom) and conduction bands (top) of a direct (left) and an indirect band gap semiconductor. The arrows indicate the magnitude of the energy band gap, E_g, the pathways of excitation of an electron from the valence band to the conduction band, electronic relaxation, fluorescence, and absorption of phonons (see text).

valence band is not an option because momentum would no longer be conserved. So, in order for diagonal recombination to happen, a phonon with matching momentum has to be absorbed during fluorescence, but because these two processes would have to happen simultaneously, this scenario is clearly a rare occurrence. As a consequence, the fluorescence lifetime from bulk crystalline silicon is very long and fluorescence intensity is very weak.

When bulk crystalline silicon is reduced in size to a scale approaching that of the nanoscale regime, translational symmetry is gradually lost. A consequence of small size of nanocrystals is, therefore, that materials that are indirect band gap semiconductors in the bulk phase become quasi-direct semiconductors at the nanoscale. For silicon, this means that high fluorescence intensities are possible if nanocrystallites are only small enough to display a quasi-direct band gap.

Another feature of such reductions in crystal size is quantum confinement. Quantum confinement relates to the shift of energy levels with size, and neatly explains the energy spectrum of, for example, color-center defects in crystals (Hayes and Stoneham 2004; Fox 2010), and electrons confined in nanoscale bubbles in liquid helium (Fowler and Dexter 1968; Grimes and Adams 1990, 1992).

These energy shifts can be understood using the popular particle-in-a-box model that is almost perennially reviewed in quantum mechanical text books. The energy spectrum, (n), of an electron confined in a one-dimensional box of length l with infinitely high box walls can be straightforwardly derived to give the following equation:

$$E(n) = \frac{n^2 \pi^2 \hbar^2}{2 m_e l^2} \tag{8.1}$$

where n is the principal quantum number, $\hbar$ the reduced Planck (or Dirac) constant, and m_e the electron mass. The quantum number, n, is indexed from 1, and the energy difference E(n = 2) and E(n = 1) would be equivalent to the fluorescence energy from the first excited state to the ground state.

The analogy of the one-dimensional model can be straightforwardly extended to three dimensions. A more realistic model, using the work function rather than infinitely high potential walls, requires solving transcendental equations. This latter, more rigorous, treatment lowers the energy values by not more than 10%, for which decreases in the energy difference and effective magnitude of the box diameter for a given transition energy are implicit. Furthermore, a more realistic potential surface than a square well would also lower the energy levels as the constraints imposed by the former must, by their very nature, be more relaxed.

Lockwood and coworkers observed that the fluorescence of an Si/SiO_2 superlattice depended on the silicon film thickness (Lockwood et al. 1996). They attributed this behavior to one-dimensional confinement of the excited electron within the silicon film. To explain the shift in the fluorescence energy, they adopted the particle-in-a-box model and showed that the peak energy of the observed red fluorescence band followed Equation 8.2.

$$E(n) = E_g + \frac{\pi^2 \hbar^2}{2 d^2}\left(\frac{1}{m_e^\star} + \frac{1}{m_h^\star}\right) \tag{8.2}$$

Here, d is the silicon layer thickness, $m_e^\star$ and $m_h^\star$ are the "effective masses" of electron and hole, although the authors acknowledge that, strictly speaking, the concept of effective electron and hole masses has no physical meaning in nanoscale systems that do not exhibit the translational symmetry of crystals. A good fit was reported for $E\,(eV)$ = 1.60 + 0.72d^{-2} eV, with d given in nm, which implies effective masses $m_e^\star \approx m_h^\star \approx$ 1 m_e in good agreement with bulk crystalline silicon were $m_e^\star(Si_{bulk})$ = 1.18 m_e and $m_h^\star(Si_{bulk})$ = 0.81 m_e. The fit shows that the band gap energy, at E_g = 1.60 eV, is considerably larger than that of bulk crystalline silicon (E_g (c-Si) = 1.12 eV at 295 K), and is, in fact, more similar to that of amorphous silicon (E_g(a-Si) = 1.5 - 1.6 eV at 295 K). The good fit with experimental data and the similarity between the confinement term in Equation 8.2 and the original particle-in-a-box Equation 8.1 is remarkable, and strongly supports the presence of quantum confinement.

Park and coworkers investigated amorphous silicon quantum dots embedded in silicon nitride. They observed fluorescence in the form of a single band whose maximum shifted with average quantum dot size. The size dependence of fluorescence energy fit to the equation was found as $E\,(eV) = 1.56 + 2.40d^{-2}$ eV, which confirmed the earlier observed band gap energy of amorphous silicon (Lockwood et al. 1996) in the limit of large dot sizes. However, the dependence on quantum confinement, $2.40d^{-2}$ eV, was much larger. The discrepancy with work conducted on Si/SiO_2 superlattices was attributed to the three-dimensional confinement of the quantum dots in silicon nitride (Park et al. 2001).

Summarizing, we have so far seen that with reduction in size of a crystal, translational symmetry is gradually lost with the consequence that indirect band gap semiconductors become quasi-direct semiconductors at the nanoscale. At the same time, the band gap energy increases because of quantum confinement.

A further important factor determining the ability to fluoresce is the electronic structure at the surface of nanocrystals. Surfaces break translational symmetry, a consequence of which is that one cannot expect the same energy band structure as might be observed for "infinite" crystals. Band gap energies may be smaller, or may not even exist. For nanocrystals, this means that surface effects may compete with quantum confinement. In the following, nonradiative decay at nanocrystal surfaces will be discussed.

To prevent nonradiative decay at its surface, a nanocrystal may be embedded in another semiconductor or insulator of larger band gap energy. This effect is illustrated in Figure 8.2.

In broadest terms, one can expect that surface effects on the band gap energy can be minimized for such a system. It is assumed that the nanocrystal structure fits well with that of the host and that a minimum of additional interface states are produced. Ideally, this would mean that an electron promoted across E_{g1} from the valence band of the nanocrystal to its conduction band would remain confined within the nanocrystal. The electron would have no other choice than to fluoresce to the ground state because no discrete states are available within the gap.

To better account for nonradiative decay in real systems, vibrational relaxation is often considered. Because of the possibility of surface reconstruction, vibrational relaxation at surfaces is particularly important for free nanoscale crystals and clusters. Figure 8.3 illustrates the cycle of excitation, electronic migration, and relaxation within the conduction band and vibrational relaxation at the surface. In this simple picture, a high density of vibrational states at the surface is assumed to exist. The electronically excited electron "finds" the surface on a subfemtosecond timescale, and relaxes by jumping down the energy ladder of vibrational states.

Another simplification implicit in this picture of a dense spectrum of vibrational states is that the short timescales of nonradiative decay are ignored. The energy level scheme shown in Figure 8.3 implies that the vibrational levels are time averages.

Under closer inspection, the consideration of relaxation pathways along such eigenstates in nanocrystals does not appear to be justified. Particularly in free clusters, the atoms at the surface can perform large amplitude vibrations. These large amplitude vibrations give rise to electronic–vibrational coupling, and open other, nonadiabatic routes for relaxation from electronically excited states to the ground state. The simple example of the triatomic, homonuclear molecule shown in Figure 8.4 illustrates this mechanism.

In this example, the molecule performs a bend vibration. At the classical turning points of this motion, structures belonging to three different point groups, $D_{\infty h}$, C_{2v}, and D_{3h}, can be identified, with the actual point group depending on the amplitude of the vibration. In other words, by performing a bend

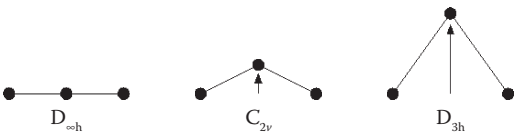

Figure 8.2 Simple schematic illustrating how vibrational–electronic coupling can lead to nonadiabatic relaxation from electronically excited states to the ground state. A linear, homonuclear triatomic molecule performing a bending vibration assumes, at various points during one such oscillation, structures that belong to three different point groups, and hence three different electronic states.

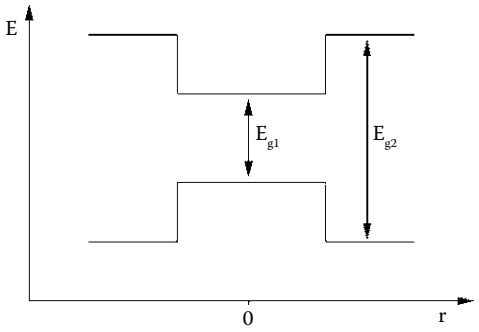

Figure 8.3 Schematic of a nanoscale crystal (quantum dot) embedded in a material of larger band gap energy. E_{g1} and E_{g2} refer to the band gap energies of the nanocrystal and host material, respectively.

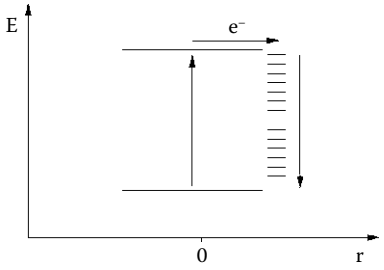

Figure 8.4 Simplified energy level diagram of a nanoscale crystal with a high density of vibrational states at its surface. The small size of the crystal means that electrons delocalized over the conduction band quickly localizing at the surface. They then relax nonradiatively by hopping across the vibrational states.

vibration, the molecule is able to intersect the different electronic states associated with these point groups. These intersection points provide passages to lower lying states.

These lower states may be dissociative. Therefore, a tendency toward isomerization and dissociation may be expected, particularly for small homonuclear clusters. This corroborates the relevance of caging through a rigid shell of atoms, moieties, or solvent molecules. In fact, deposition of metal clusters into argon matrices and argon droplets has made the observation of photoluminescence possible (Felix et al. 2001; Sieber et al. 2004; Conus et al. 2006; Harbich et al. 2007). Argon shells have also been used to cage oxygen molecules; the observed luminescence was attributed to oxygen atoms that had first dissociated but were then forced, by the cage, to recombine (Laarmann et al. 2008).

In summary, nonadiabatic decay at the surface of homonuclear clusters is an important relaxation channel in terms of its competition with fluorescence. The design and engineering of fluorescent clusters therefore requires that this possibility be suppressed. In broadest terms, the passivation of dangling bonds at a surface with atoms such as hydrogen (hydrides), halogens (halides), oxygen (oxides), or molecular groups such as alkenes, amines, or polymers can be understood to confine the electronically excited electron to the core region of the cluster. The distinctly higher fluorescence intensities that arise from this confinement can be observed. This was confirmed by Seraphin and coworkers (Seraphin et al. 1996), who investigated silicon nanoparticles produced by laser ablation with and without passivation, in vacuo. They found that passivation increased fluorescence intensity, but left the fluorescence energy itself unchanged. Embedding clusters and nanocrystals within a lattice-matching host of a larger band gap energy fulfills the same purpose. Also, in the ideal case of a lattice-matching interface, large amplitude vibrations would be successfully suppressed purely as, though not necessarily limited to, a matter of sterics. Passivated or core-shell clusters embedded in a solvent can also effectively transfer and absorb excess vibrational energy.

8.3 CLUSTERS

Clusters are understood as being particles consisting of as few as two, three, or four, or as having as many as a few thousand, atoms. The term "cluster" is used alongside the term "nanoparticles," but clusters are commonly understood to represent smaller particles. The study of clusters is motivated by the desire to understand the often dramatic changes of material properties that accompany changes in size. Material properties also depend on structure and dimensionality, and similarly accompany changes in size. All such characteristics are relevant in cluster science research.

8.3.1 PRODUCTION OF SILICON CLUSTERS

Free clusters are frequently studied in supersonic beams. A gas under high pressure is expanded through a tiny aperture into vacuum. During expansion, it cools and nucleates via removal of excess energy through three-body collisions, forming clusters. They fly through vacuum where they can, for instance, be investigated free from external interactions, or can otherwise be deposited on a substrate. For silicon clusters, this production method is unsuitable because it requires atomic vapor of significant pressure. Silicon has a comparably low vapor pressure, even at high temperatures, rendering supersonic expansion of thermally produced silicon vapor through a nozzle into vacuum an unrealistic mechanism for silicon cluster production.

Supersonic beams have been employed in sources where silicon has been generated by decomposition of precursor gases which are then mixed with a carrier/aggregation gas. Silane diluted in helium and exposed to a discharge has been expanded through a pulsed piezoelectric valve (Hoops et al. 2001). Ehbrecht and Huisken (1999) used a pulsed CO_2 laser to decompose silane diluted in helium. The products were expanded into vacuum and subsequently investigated by time-of-flight mass spectrometry or deposited onto CF_2 or LiF substrates (Ehbrecht et al. 1997).

Silicon clusters have been produced using the principle of gas aggregation (Sattler et al. 1980). Silicon vapor is mixed with a "seeding" gas, which induces the three-body collisions required for nucleation. It also facilitates growth by mediating collisions between silicon atoms and removing the latent heat that is released during any subsequent growth of clusters from these collisions.

To generate silicon vapor within a seed gas, laser vaporization, sputtering, and pulsed arcs have been used. Laser vaporization sources employ pulsed laser sources that are fired at a rotating silicon rod (Bloomfield et al. 1985; Jarrold and Constant 1991; Bower and Jarrold 1992; Honea et al. 1993a, 1999). Sputter gas aggregation sources employ a modified sputter electrode configuration, allowing higher operating gas pressures than are usually needed in sputtering for thin film production (Haberland et al. 1991; Hoffmann et al. 2001b; Pratontep et al. 2005; Wegner et al. 2006; von Haeften et al. 2009). Argon and helium are used as seed gases. Helium produces smaller clusters because it is much lighter than silicon and energy transfer is less efficient. The pulsed arc cluster ion source is another variation of a gas aggregation-type cluster source that has been used for silicon cluster production (Maus et al. 2000).

These sources produce neutral and ionic clusters, including both cations and anions; charged clusters can be easily manipulated in a spatial sense via electrostatics, and can therefore be mass selected. Kitsopoulos and coworkers size-selected silicon cluster anions, which were then photoexcited into the neutral ground state as well as other low-lying electronically excited states of the neutral clusters by the process of electron detachment (Kitsopoulos et al. 1990). Honea and coworkers used arrangements of linear and perpendicular quadrupole mass selectors to size-select silicon cluster ions and deposit them onto a surface (Honea et al. 1999). To soften the impact, rare gas buffer layers were codeposited onto a cold, predeposited rare gas matrix (Honea et al. 1999). A similar scheme was used by Grass and coworkers, who soft-landed Si_4 on highly oriented pyrolytic graphite (HOPG) and performed X-ray photoelectron spectroscopy (Grass et al. 2002). Astruc Hoffmann and coworkers used a reflectron time-of-flight (RETOF) mass spectrometer in combination with a multiwire mass gate to size-select silicon anion clusters on which to subsequently perform photoelectron spectroscopy. The size-selected clusters were irradiated with UV light from an ArF excimer laser and analyzed in a magnetic bottle photoelectron spectrometer (Hoffmann et al. 2001b).

Hirsch and coworkers introduced size-selected silicon clusters into an ion trap (Hirsch et al. 2009; Lau et al. 2011; Vogel et al. 2012; Kasigkeit et al. 2015). The trapped clusters were excited by monochromatic synchrotron radiation, allowing the determination of core-level shifts for specific cluster sizes.

8.3.2 GEOMETRIC STRUCTURE

A great variety of geometric structures have been reported for silicon clusters using both theoretical and experimental methods. In general, it has been found that the structures of neutral, cation, and anion cluster species differ considerably. Anions have frequently been used to elucidate electronic and geometric features. Their structures are affected by Jahn–Teller distortions. Care must be taken when compared to neutral clusters.

In a number of early studies, silicon clusters produced using supersonic beam techniques were deposited and investigated spectroscopically. Honea and coworkers deposited size-selected silicon clusters into argon, krypton, and nitrogen matrices using codeposition onto a liquid helium-cooled substrate (Honea et al. 1993b, 1999). Using surface plasmon polariton-enhanced Raman spectroscopy, sharp features characteristic of Si_4, Si_6, and Si_7 structures were identified in their spectra, which were in good agreement with earlier *ab initio* calculations (Raghavachari and Logovinsky 1985; Raghavachari 1986; Tománek and Schlüter 1986; Raghavachari and Rohlfing 1988; Ballone et al. 1988). The spectra also revealed evidence for the presence of cluster–cluster aggregation within the rare gas matrix. The spectra of the aggregates of Si_4, Si_6, and Si_7 bore considerable similarities to those of larger clusters, such as Si_{25-35}, as well as those of amorphous silicon (Honea et al. 1999).

The structure of free silicon clusters in the size range from n = 10 to n = 100 was addressed using drift mobility measurements, the results of which revealed a prevalence for prolate-shaped structures. A structural transition occurs at sizes around n = 27; however, larger clusters were found to prefer more spherical configurations (Jarrold and Constant 1991). The preference for prolate shapes was attributed to a tendency of the silicon atoms to minimize coordination. This trend competes with the surface energy of the clusters, ultimately leading to a preference for spherical structural motifs in larger clusters (Jarrold and Constant 1991). The experiments were repeated at higher resolution (Hudgins et al. 1999), and calculations confirm these experimental findings (Ho et al. 1998; Jackson et al. 2004).

Vibrational spectroscopy of anions has been performed by photoexcitation spectroscopy into the neutral state using electron detachment (Kitsopoulos et al. 1990; Xu et al. 1998). Comparison of the resultant spectral features with calculations reveals the structures of the anions. Recent work on larger silicon cluster anions reveals vibrational spectra indicative of the previously observed transition from prolate to spherical shapes (Meloni et al. 2004).

The FELIX free electron laser source provides intense and tunable infrared radiation including in the spectral range from 166 to 600 cm^{-1} where silicon clusters absorb. Vibrational spectroscopy of small silicon cluster cations was performed using multiple photon dissociation spectroscopy. The ions were analyzed in a time-of-flight mass spectrometer. Also, isotopically selected ^{129}Xe atoms were attached to the clusters. Absorption of multiple IR photons would lead to a depletion of the ion signal, allowing the requisition of spectra of size-selected clusters. Comparison of the spectra with calculations using density functional theory (DFT) revealed novel structures and a growth motif that started with a pentagonal bipyramid building block and changed to a trigonal prism for larger clusters (Lyon et al. 2009).

Related work provided information on the structure of small neutral silicon clusters (Fielicke et al. 2009). Using a combination of tunable far-infrared radiation from the FELIX free-electron laser source and vacuum-ultraviolet two-color ionization, it was possible to scan the spectrum of homonuclear neutral silicon clusters in the spectral range from 200 to 550 cm^{-1}. The use of vacuum-ultraviolet two-color ionization provided the advantage of detection of the initially neutral clusters with mass selectivity. An increase of the ionization rate was observed when IR photons had been absorbed. Comparison with DFT and Møller–Plesset (MP2) perturbation theory calculations revealed that the ground-state potential energy surface was very flat. Therefore, rapid interconversion between different structures might well be expected, as well as the presence of higher energy isomers in real-world experimental samples (Fielicke et al. 2009).

Furthermore, theoretical work suggested that, at intermediate sizes, around 20 atoms silicon clusters tend to build irregular cages stabilized by a small number of encapsulated silicon atoms (Mitas et al. 2000). Silicon cages can also be stabilized by encapsulated foreign atoms (Kumar and Kawazoe 2001, 2003a, 2003b). Stable hollow structure similar to C_{60} buckminsterfullerene (buckyballs), can nevertheless be excluded (Sun et al. 2003).

In summary, the structures of silicon clusters grown in the gas phase differ from the structures of silicon nanocrystals that have been produced, for example, by etching of bulk crystalline silicon. The structures of small silicon clusters are characterized by the tendency of the atoms to minimize coordination, thereby favoring growth of prolate shapes. Therefore, their bond angles are smaller than their counterparts in sp^3 bonded, cubic diamond-structured bulk silicon. The consequences of this behavior are shorter internuclear separations and higher atomic densities. An exemption from these principles is shown in the work of Laguna and coworkers, however, who deposited silicon clusters produced by pyrolysis of silane onto holey carbon films. High-resolution transmission electron images clearly show nanoparticles with lattice planes surrounded by an amorphous oxide shell (Hofmeister et al. 1999; Laguna et al. 1999).

8.3.3 ELECTRONIC STRUCTURE

Photoelectron spectra of silicon cluster anions have frequently been reported in the literature. These spectra exhibit rich features for small clusters, which become smoother as the clusters become larger. Maus et al. (2000) assign the low-binding energy features to the extra electron occupying the conduction bands. The higher-energy features observed are attributed to the valence electrons. The energy difference between the two corresponds to the band gap in the bulk picture. Small clusters between n = 3 and 13 were found to have band gap energies smaller than those typically seen for bulk crystals (Maus et al. 2000). This is incommensurate with the idea of quantum confinement, which would predict larger band gap energies for anything smaller than the bulk. The results were attributed to the entire geometric and electronic structure being affected by surface effects, similar to the reconstruction of the surface of bulk silicon crystals. While such an effect must clearly dominate the electronic structure of small clusters, the trend continues for larger clusters as well; Hoffmann et al., for instance, report the absence of a band gap for clusters up to 1000 atoms (Hoffmann et al. 2001a). For large Si cluster anions, the photoelectron spectrum is dominated by a single smooth and broad feature. The onset of photoemission shifts with size toward larger binding energies, a trend that is incommensurate with a bulk band gap picture and contrary to what one would expect from quantum confinement.

The observations made through photoelectron spectroscopy of cluster anions in free beams match measurements of band gap energies of silicon clusters deposited on HOPG (Marsen et al. 2000). Such band gap energies were always smaller than those of their bulk counterparts, which agrees with a different geometric structure than the diamond cubic structure of the bulk. Also, a transition region was found for sizes around 1.5 nm, corresponding to 44 atoms; larger clusters had no band gap.

Band gap energies of cationic VSi_n^+ were determined by X-ray spectroscopy using monochromatic synchrotron radiation and an ion trap to store the size-selected clusters (Lau et al. 2011). By measuring the ion yield of specific ion decay channels, it was possible to record a direct 2p photoionization spectrum separately from the resonant 2p photoionization spectrum, yielding the energy difference E_{XAS} between the core level and the lowest unoccupied molecular orbital (LUMO), and E_{CL}, the energy difference between the core and the vacuum level, E_{VAC}. Measurement of the valence state photoionization spectrum E_{VB} yields the difference between the highest occupied molecular orbital (HOMO) and the the vacuum level, E_{VAC}. For the band gap energy, E_g, or, more precisely, the HOMO–LUMO energy difference, it follows $E_g = E_{VB} - E_{CL} + E_{XAS}$.

Photoionization thresholds were measured for silicon clusters in the size range from n = 2 to 200 using laser photoionization with RETOF mass spectrometry detection (Fuke et al. 1993). The ionization potential revealed features that were ascribed to a structural transition for sizes around n = 20. Measurements of the 2p core level and valence electron binding energies using monochromatic synchrotron radiation and an ion trap show a similar size dependence (Vogel et al. 2012). Both 2p binding energy and ionization potential show a linear dependence on the inverse cluster radius $n^{-1/3}$. Such a dependence is expected from the size-dependent charging energy, similar to metal clusters (Halder and Kresin 2015). Furthermore, core-level shifts were derived and compared to *ab initio* calculations (Vogel et al. 2012).

8.4 FLUORESCENT SILICON CLUSTERS

The electronic level structure associated with dense packing, suggesting very small band gap energies for small- and medium-sized silicon clusters and even the absence of band gaps, is unfavorable toward fluorescence. Indeed, fluorescence from free silicon clusters in traps or in molecular beams has not yet been reported in the literature. The work on neutral and cationic silver clusters in argon droplets and solid matrices (Felix et al. 2001; Sieber et al. 2004; Conus et al. 2006; Harbich et al. 2007) suggests that fluorescence might be possible if silicon clusters are deposited and embedded in rare gas matrices. While such deposition experiments have been carried out (Honea et al. 1993b, 1999), attempts to observe fluorescence with this setup are not known to the author.

It appears that fluorescence reported for nanoscale silicon can be attributed to the effects of quantum confinement, passivation, and the presence of defects. To achieve confinement, passivation, or defects due to other materials, molecules, or atoms are actively introduced. In the vast majority of bottom-up methods used to produce fluorescent silicon nanoparticles, chemical methods are employed. Exceptions are laser vaporization of silicon targets in liquids (Švrček et al. 2009a; Švrček et al. 2009b; Alkis et al. 2012; Intartaglia et al. 2012a; Švrček et al. 2016; Rodio et al. 2016), pyrolysis of silane in gas-flow reactors (Ehbrecht et al. 1997) and silicon cluster codeposition with water vapor (von Haeften et al. 2009).

8.5 RED–ORANGE LUMINESCENCE

Silicon clusters produced by CO_2 laser-induced decomposition of silane were found to show red photoluminescence after they were deposited onto LiF or CaF_2 substrates, and transferred to ambient air (Ehbrecht et al. 1997). Owing to a continuous supersonic beam and a pulsed CO_2 laser, the part of the beam containing clusters was also pulsed. A velocity selector was employed to select velocity segments of the cluster pulse, and the cluster mass was measured by time-of-flight mass spectrometry (Ledoux et al. 2002). The average number of atoms in the clusters, $\bar{N}$, was found to vary from $\bar{N} = 395$, corresponding to an average diameter, $\bar{D}$, of 2.47 nm to $\bar{N} = 9070$, corresponding to $\bar{D} = 7.03$ nm. The diameters were deduced using a spherical particle model,

$$D(N) = \left(\frac{3N}{4\pi} V_{unit} \right)^{1/3} \tag{8.3}$$

where $V_{unit} = 0.1601$ nm^3 is the volume of the unit cell of bulk crystalline silicon. Equation 8.3 takes into account the fact that the unit cell has a diamond cubic structure and contains eight atoms. It is assumed that bulk and nanoparticle densities are the same.

These samples were photoexcited at 488 nm using continuous laser radiation, and the resultant fluorescence spectrum was measured. Each sample showed an almost symmetric fluorescent band whose peak wavelength decreased with particle diameter. The size-dependent fluorescence wavelength shifts agreed with the results one might anticipate from quantum confinement. Deviations were attributed to partial oxidation of the surface layer, which could also be seen in high-resolution transmission electron microscopy (HRTEM) images (Laguna et al. 1999). The oxide shell thickness could be correlated linearly to the cluster diameter. The smallest clusters of 6 nm in diameter had an oxide shell with a thickness of 0.81 nm, while the largest particles had a diameter of 34 nm and a 3 nm thick oxide shell (Hofmeister et al. 1999). The HRTEM images showed that the nanoparticles had a crystalline core. A number of different silicon lattice planes were identified from diffraction rings.

Hofmeister and coworkers also investigated the spacing of a (111) lattice as a function of cluster size. They found that large silicon clusters exhibited compressed (111) lattices compared to bulk crystalline silicon. However, clusters smaller than 3 nm in diameter were found to be dilated. The dependence of the (111) lattice spacing on the cluster diameter followed:

$$d(111) = \frac{0.023}{D} + 0.307[\text{nm}] \tag{8.4}$$

where D is the cluster diameter.

Because the photoluminescence of silicon was found to depend on pressure, the authors concluded that the size-dependent lattice separation must be taken into account in a modified equation for the photoluminescence energy caused by quantum confinement (Ledoux et al. 2000).

$$E_{PL}^{corr} = E_0 + \frac{3.73}{D^{1.39}} + \frac{0.881}{D} - 0.245 \tag{8.5}$$

Here, E_{PL}^{corr} is the energy of the photoluminescent band, as corrected for size-dependent lattice separation, in eV. E_0 is the band gap energy of bulk crystalline silicon at room temperature (1.17 eV) (Ledoux et al. 2000).

It is important to note that all samples had been transferred to air testing for photoluminescence. The samples were kept in an argon atmosphere during transfer (Ehbrecht et al. 1997). After production and exposure to air, the crystalline core section of the particles was found to reduce in diameter (Ledoux et al. 2000, 2001). Also, the photoluminescence energy was found to blue shift, which was attributed to the smaller sizes of the silicon clusters, supporting the assertion that quantum confinement was controlling fluorescence properties (Ledoux et al. 2001). The effect of quantum confinement was also investigated by etching the oxide layer using hydrofluoric acid (HF). This was found to narrow the spectral band width of the luminescence but not the peak wavelength, since the silicon crystalline core itself would clearly not be affected by such treatment with HF. The effect of passivation on the fluorescence intensity, but not on the fluorescence wavelength, is in line with earlier work by Seraphin and coworkers (Seraphin et al. 1996).

Pyrolysis of silane in vacuum was also used by Li and coworkers to produce silicon clusters (Li et al. 2004a, 2004b), who post-processed the samples by etching with HF and nitric acid (HNO_3). This was found to reduce the cluster size and the intensity of visible luminescence.

8.6 BLUE FLUORESCENCE

To investigate the effect of passivation of silicon clusters *in situ*, von Haeften and coworkers used a molecular beam codeposition scheme (von Haeften et al. 2009). They produced silicon clusters by gas aggregation using ion sputtering in an argon–helium atmosphere, codepositing them with a beam of water vapor onto a liquid nitrogen-cooled target. After a deposition time of 30 minutes, the target was warmed up, whereupon the ice-silicon mixture melted and a few milliliters of liquid sample was collected. A schematic of the apparatus used is shown in Figure 8.5.

When photoexcited with 308 nm UV light, all liquid samples showed a blue fluorescence that peaked at 420 nm (von Haeften et al. 2009). The fluorescence intensity was stable over several months (Brewer and von Haeften 2009). When the photoexcitation wavelength was decreased from 310 to 240 nm, the wavelength of the fluorescent band remained at 420 nm; however, additional fluorescence bands appeared in the UV region (von Haeften et al. 2010a, 2010b; Torricelli et al. 2011). When the clusters were embedded

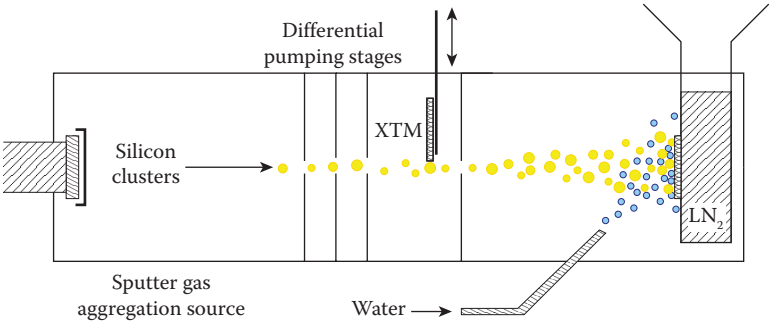

Figure 8.5 Schematic of experimental setup used by von Haeften et al. (2009); Brewer and von Haeften (2009); Torricelli et al. (2011).

in liquid ethanol and isopropanol, the fluorescence wavelength shifted to 365 and 380 nm, respectively (Galinis et al. 2012b). The fluorescence lifetime was measured using monochromatic synchrotron radiation. For an excitation wavelength at 195 nm and fluorescence at 300 nm, a lifetime of 3.7 ns was determined (Yazdanfar et al. 2012).

Time-correlated fluorescence spectroscopy showed that the blue fluorescence consisted of at least two components: the spectral component with a long fluorescent lifetime that peaked at 2.7 eV (Yazdanfar et al. 2012), which is a perfect match with the fluorescence of defect-rich silica (Skuja et al. 1984), and a second short-lived, and much more intense, component, which peaked at 3.0 eV (Yazdanfar et al. 2012). The good energy match and the long lifetime of the first of these bands suggested it arose due to the spin-forbidden $T_1 \rightarrow S_0$ transition observed for twofold coordinated Si in SiO_2 (O-Si-O) (Skuja et al. 1984; Skuja 1992; Nishikawa et al. 1992; Fitting et al. 2004).

Short lifetimes have frequently been reported for the blue fluorescence of nanoscale silicon (Kovalev et al. 1994). Tsybeskov and coworkers investigated the lifetime of blue fluorescence emitted from thermally and chemically oxidized porous silicon (Tsybeskov et al. 1994). The decay was multiexponential with a lifetime of ~1 ns, which was independent of the excitation energy. Furthermore, the appearance of blue fluorescence was correlated to the presence of silicon oxide. Silicon-hydrogen bonds were absent.

Harris and coworkers prepared blue light-emitting silicon samples by electrochemical etching. They found that the samples rapidly degraded, but were able to measure photoluminescence spectra at a sample temperature of 120 K; both red- and blue-emitting components were observed. Fluorescence decay of the blue fluorescence was measured at 77 K as having a time constant of 0.86 ns. The decay was monoexponential (Harris et al. 1994).

By using different post-processing chemical treatments, porous silicon can be prepared to emit either blue or red fluorescence. Žídek and coworkers used such methods to measure the luminescence decay time separately for the two different wavelength ranges. They found that both types of fluorescence have distinct characteristics in their ultrafast decay time. The blue fluorescent band is attributed to several underlying bands which vary further, depending on sample preparation (Žídek et al. 2011).

Light emission in the blue spectral range is a known phenomenon for colloidal suspensions of silicon nanoparticles (Kimura 1999; Belomoin et al. 2000; Valenta et al. 2008) and silicon nanocrystal films (Loni et al. 1995; Canham et al. 1996; de Boer et al. 2010; Ondič et al. 2014). At the present time, there seems to be a consensus that the vast majority of reported fluorescent bands in the blue spectral range are due to localized transitions, rather than being caused by quantum confinement (Dasog et al. 2013, 2016). The precise nature of this fluorescence is nevertheless debated, though it is nevertheless reasonable to attribute it to a range of different transitions which have similar transition energies.

To elucidate the nature of the blue fluorescence, various sample preparation techniques have been explored. Responses to various chemical treatments and correlation to fluorescence performance, as well as chemical analysis, have been employed. The results are not always consistent.

Konkievicz and coworkers prepared porous silicon films and investigated photoluminescence over a wide spectral range. Under photoexcitation with 193 nm excimer laser radiation, they observed red luminescence. After annealing in an oxygen atmosphere with 2% organochlorine, blue luminescence around 400 nm appeared. The blue band appeared at annealing temperatures of 750°C and increased in intensity up to temperatures of 150°C, after which no further increases were seen (Kontkiewicz et al. 1994). Fourier transform infrared (FT-IR) measurements showed the presence of silicon oxide. This preparation was also repeated in a nitrogen atmosphere. Annealing in nitrogen did not produce blue luminescence. This led to the conclusion that the blue luminescence originates from oxidized nanostrutured silicon, although later work showed a correlation between blue fluorescence intensity and nitrogen content (Dasog et al. 2013). Results similar to those of Konkievicz and coworkers have also been reported from porous Si that was oxidized and annealed at 880°C (Kanemitsu et al. 1994). Depending on the production method, the band maxima range from 400 to 460 nm (Yu et al. 1998). The specific response of red and blue luminescence intensity to repeated etching and oxidation was investigated by Lockwood and coworkers, leading them to the conclusion that, at least, quantum confinement cannot be responsible for the blue luminescence (Lockwood et al. 1996).

An important aspect of chemical treatment is how silicon nanoparticles interact with an aqueous environment. This is because water is a strong oxidizing agent, but also because of the relevance of

nanoparticles to biomedical applications. Water may also be expected to quench fluorescence because of its dense vibrational spectrum. The interaction with water has been found to chemically modify silicon nanoparticles, and as a consequence its fluorescence activity has been seen to "degrade" (Li and Ruckenstein 2004; Erogbogbo and Swihart 2007; Erogbogbo et al. 2008). However, blue fluorescence from nanoscale silicon has been frequently observed, specifically in connection with treatment with water (Švrček et al. 2009a; Švrček et al. 2009b, 2016; Alkis et al. 2012; Intartaglia et al. 2012a, 2012b; Rodio et al. 2016).

Hou and coworkers treated light-emitting porous silicon with boiling water (Hou et al. 1993) and observed a large blue shift in the fluorescence toward the green–blue spectral range. Infrared spectroscopy was performed with the specific goal to assess whether the formation of silicon monohydride (2080 cm^{-1}) and silicon dihydride (2120 cm^{-1}) was correlated with the appearance of blue fluorescence. Prior to treatment with water, both lines were present in the spectrum and decreased in intensity after boiling water was added. Instead, a band appeared at 1105 cm^{-1}, showing that treatment with water had caused oxidation (Hou et al. 1993).

Koyama and coworkers annealed oxidized porous silicon in water vapor and observed a drastic enhancement in the blue fluorescence intensity (Koyama et al. 1998). Infrared absorption spectroscopy indicated that this annealing increased the absorption peaks related to OH vibrations except for those of free silanol, which disappeared completely. No traces of carbon-related signals were observed, contrary to the previously suspected involvement of carbon (Kontkiewicz et al. 1994; Canham et al. 1996).

Many authors report that the emission of blue fluorescence is correlated with very small structures, perhaps only a few nanometers in size. Akcakir and coworkers etched p-type boron-doped silicon using H_2O_2 and HF (Yamani et al. 1997; Akcakir et al. 2000). The combined effect of the two chemicals produced exceptionally small structures, which were then dispersed in acetone. Under photoexcitation at 355 nm, blue fluorescence was observed. Using two-photon excitation with 780 nm light pulses of 150 fs duration, fluorescence correlation spectroscopy (FCS) was performed, which suggested a hydrodynamic radius of 0.9 nm (Akcakir et al. 2000). The same research group presented TEM images of graphite films coated with this colloidal solution. The images showed agglomerated particles of 1 nm in diameter, in very good agreement with the FCS work (Belomoin et al. 2000). IR spectra showed various Si–H bands of the freshly prepared samples: 520–750 cm^{-1} (SiH_2 scissors or SiH_3), 880–900 cm^{-1} (Si–H wagging), and 2070–2090 cm^{-1} (SiH stretch and coupled H–Si–Si–H). The 1070 cm^{-1} Si–O stretch was also observed. Treatment with H_2O_2 and subsequent IR spectroscopy was found to replace first the di- and trihydrogen bonds and then the Si–H with Si–O. The coupled H–Si–Si–H bonds showed somewhat greater resilience. The blue fluorescence intensity changed by no more than a factor of two after H_2O_2 treatment (Belomoin et al. 2000).

Fluorescent silicon clusters produced by codeposition with water vapor onto a cold target showed similar sizes. Atomic force microscopy in noncontact and constant force mode of cluster films produced by drop-casting colloidal solution onto freshly cleaved HOPG showed uncovered regions of graphite, and agglomerated monolayers, as well as double layers, of clusters (Torricelli et al. 2011). The height of the monolayers reflected the difference of the tip-HOPG and tip-cluster forces, and hence cannot be taken as a measure of cluster height. However, measuring the differences between the tip-first cluster and tip-second cluster layers was expected to give a fair estimate of the height of the clusters in the film. Values between 0.92 and 1.62 nm were found (Galinis et al. 2012a), in very good agreement with Belomoin and coworkers (Belomoin et al. 2000).

Further studies using chemically produced silicon nanoparticles confirm the relation between blue luminescence, small cluster sizes, and localized transitions. Zhong and coworkers report XRD diffraction peaks similar to the diamond structure of bulk crystalline silicon (Zhong et al. 2013). Size distributions were measured by TEM, for which an average size of 2.2 nm was found (Zhong et al. 2013). Li and coworkers observed very high quantum yields of blue fluorescence, up to 75%, which were attributed to surface treatment with nitrogen-containing agents (Li et al. 2013). Furthermore, Li showed that the fluorescence wavelength can be tuned by different ligands attached to nitrogen-capped silicon clusters (Li et al. 2016). Also, the quantum yield could be increased further, up to 90%, and the emission bandwidth could be narrowed. They attribute their observations to localized transitions at the cluster surface and propose a "ligand law" controlling the photoluminescence (Li et al. 2016).

8.7 CONCLUSIONS

Silicon clusters consisting of a small number of atoms are fascinating objects through which one can study the evolution of material properties with complexity and size. Free clusters produced in molecular beams have properties that are unfavorable for light emission. However, when passivated or embedded in a suitable host, they may emit fluorescence. The current available data show that both quantum confinement and localized transitions, often at the surface, are responsible for fluorescence. By building silicon clusters atom by atom, and by embedding them in shells atom by atom, new insights into the microscopic origins of fluorescence from nanoscale silicon can be expected.

The methods needed to perform such experiments, such as spectroscopy in droplets of argon (Felix et al. 2001) and helium (Feng et al. 2015; Katzy et al. 2016), have recently been developed. It can be hoped that they will be used for the study of fluorescence of silicon clusters. In view of the rising number of studies of fluorescent silicon nanostructures for biomedical and other applications (Dasog et al. 2014; McVey and Tilley 2014), the value and importance of such studies is clear.

REFERENCES

Akcakir, O., Therrien, J., Belomoin, G., Barry, N., Muller, J. D., Gratton, E., and Nayfeh, M. (2000). Detection of luminescent single ultrasmall silicon nanoparticles using fluctuation correlation spectroscopy. *Appl. Phys. Lett.*, 76(14):1857–1859.

Alkis, S., Okyay, A. K., and Ortaç, B. (2012). Post-treatment of silicon nanocrystals produced by ultra-short pulsed laser ablation in liquid: Toward blue luminescent nanocrystal generation. *J. Phys. Chem. C*, 116(5):3432–3436.

Ballone, P., Andreoni, W., Car, R., and Parrinello, M. (1988). Equilibrium structures and finite temperature properties of silicon microclusters from ab initio molecular-dynamics calculations. *Phys. Rev. Lett.*, 60(4):271.

Belomoin, G., Therrien, J., and Nayfeh, M. (2000). Oxide and hydrogen capped ultrasmall blue luminescent Si nanoparticles. *Appl. Phys. Lett.*, 77:779.

Belomoin, G., Therrien, J., Smith, A., Rao, S., Twesten, R., Chaieb, S., Nayfeh, M., Wagner, L., and Mitas, L. (2002). Observation of a magic discrete family of ultrabright Si nanoparticles. *Appl. Phys. Lett.*, 80(5):841–843.

Bloomfield, L. A., Freeman, R. R., and Brown, W. L. (1985). Photofragmentation of mass-resolved clusters. *Phys. Rev. Lett.*, 54(20):2246–2249.

Borsella, E., Botti, S., Cremona, M., Martelli, S., Montereali, R., and Nesterenko, A. (1997). Photoluminescence from oxidised Si nanoparticles produced by CW CO_2 laser synthesis in a continuous-flow reactor. *J. Mater. Sci. Lett.*, 16(3):221–223.

Bower, J. E., and Jarrold, M. F. (1992). Properties of deposited size-selected clusters: Reactivity of deposited silicon clusters. *J. Chem. Phys.*, 97(11):8312–8321.

Brewer, A., and von Haeften, K. (2009). In-situ passivation and blue luminescence of silicon clusters using a cluster beam/H_2O co-deposition production method. *Appl. Phys. Lett.*, 94:261102.

Brus, L., Szajowski, P., Wilson, W., Harris, T., Schuppler, S., and Citrin, P. (1995). Electronic spectroscopy and photophysics of Si nanocrystals: Relationship to bulk c-Si and porous Si. *J. Am. Chem. Soc.*, 117(10):2915–2922.

Canham, L. (2000). Gaining light from silicon. *Nature*, 408:411–412.

Canham, L., Loni, A., Calcott, P., Simons, A., Reeves, C., Houlton, M., Newey, J., Nash, K., and Cox, T. (1996). On the origin of blue luminescence arising from atmospheric impregnation of oxidized porous silicon. *Thin Solid Films*, 276(1):112–115.

Canham, L. T. (1990). Silicon quantum wire array fabrication by electrochemical and chemical dissolution of wafers. *Appl. Phys. Lett.*, 57:1046–1048.

Cheng, X., Lowe, S. B., Reece, P. J., and Gooding, J. J. (2014). Colloidal silicon quantum dots: From preparation to the modification of self-assembled monolayers (SAMs) for bio-applications. *Chem. Soc. Rev.*, 43(8):2680–2700.

Chinnathambi, S., Chen, S., Ganesan, S., and Hanagata, N. (2014). Silicon quantum dots for biological applications. *Adv. Health. Mat.*, 3(1):10–29.

Choi, J., Zhang, Q., Reipa, V., Wang, N. S., Stratmeyer, M. E., Hitchins, V. M., and Goering, P. L. (2009). Comparison of cytotoxic and inflammatory responses of photoluminescent silicon nanoparticles with silicon micron-sized particles in RAW 264.7 macrophages. *J. Appl. Toxicol.*, 29(1):52–60.

Conus, F., Rodrigues, V., Lecoultre, S., Rydlo, A., and Félix, C. (2006). Matrix effects on the optical response of silver nanoclusters. *J. Chem. Phys.*, 125:024511.

Cullis, A., and Canham, L. (1991). Visible light emission due to quantum size effects in highly porous crystalline silicon. *Nature*, 353(6342):335–338.

Cullis, A., Canham, L., and Calcott, P. (1997). The structural and luminescence properties of porous silicon. *J. Appl. Phys.*, 82:909–965.

Dasog, M., De los Reyes, G. B., Titova, L. V., Hegmann, F. A., and Veinot, J. G. (2014). Size vs surface: Tuning the photoluminescence of freestanding silicon nanocrystals across the visible spectrum via surface groups. *ACS Nano*, 8(9):9636–9648.

Dasog, M., Kehrle, J., Rieger, B., and Veinot, J. G. (2016). Silicon nanocrystals and silicon-polymer hybrids: Synthesis, surface engineering, and applications. *Angew. Chem. Int. Ed.*, 55(7):2322–2339.

Dasog, M., Yang, Z., Regli, S., Atkins, T. M., Faramus, A., Singh, M. P., Muthuswamy, E., Kauzlarich, S. M., Tilley, R. D., and Veinot, J. G. (2013). Chemical insight into the origin of red and blue photoluminescence arising from free-standing silicon nanocrystals. *ACS Nano*, 7(3):2676–2685.

de Boer, W., Timmerman, D., Dohnalová, K., Yassievich, I., Zhang, H., Buma, W., and Gregorkiewicz, T. (2010). Red spectral shift and enhanced quantum efficiency in phonon-free photoluminescence from silicon nanocrystals. *Nat. Nanotechnol.*, 5:878.

Dohnalová, K., Gregorkiewicz, T., and Kusová, K. (2014). Silicon quantum dots: Surface matters. *J. Phys.*, 26(17):173201.

Echt, O., Sattler, K., and Recknagel, E. (1981). Magic numbers for sphere packings: Experimental verification in free xenon clusters. *Phys. Rev. Lett.*, 47(16):1121–1124.

Ehbrecht, M., and Huisken, F. (1999). Gas-phase characterization of silicon nanoclusters produced by laser pyrolysis of silane. *Phys. Rev. B*, 59(4):2975–2985.

Ehbrecht, M., Kohn, B., Huisken, F., Laguna, M. A., and Paillard, V. (1997). Photoluminescence and resonant Raman spectra of silicon films produced by size-selected cluster beam deposition. *Phys. Rev. B*, 56(11):6958–6964.

Erogbogbo, F., and Swihart, M. T. (2007). Photoluminescent silicon nanocrystals with mixed surface functionalization for biophotonics. *Mater. Res. Soc. Symp. Proc.*, 958:239.

Erogbogbo, F., Yong, K., Roy, I., Xu, G., Prasad, P., and Swihart, M. (2008). Biocompatible luminescent silicon quantum dots for imaging of cancer cells. *ACS Nano*, 2(5):873–878.

Erogbogbo, F., Yong, K.-T., Roy, I., Hu, R., Law, W.-C., Zhao, W., Ding, H., et al. (2010). In vivo targeted cancer imaging, sentinel lymph node mapping and multi-channel imaging with biocompatible silicon nanocrystals. *ACS Nano*, 5(1):413–423.

Falconieri, M., Borsella, E., De Dominicis, L., Enrichi, F., Franzò, G., Priolo, F., Iacona, F., Gourbilleau, F., and Rizk, R. (2005). Probe of the Si nanoclusters to Er energy transfer dynamics by double-pulse excitation. *Appl. Phys. Lett.*, 87:061109.

Felix, C., Sieber, C., Harbich, W., Buttet, J., Rabin, I., Schulze, W., and Ertl, G. (2001). Ag_8 fluorescence in argon. *Phys. Rev. Lett.*, 86(14):2992–2995.

Feng, C., Latimer, E., Spence, D., Al Hindawi, A. M., Bullen, S., Boatwright, A., Ellis, A. M., and Yang, S. (2015). Formation of Au and tetrapyridyl porphyrin complexes in superfluid helium. *Phys. Chem. Chem. Phys.*, 17(26):16699–16704.

Fielicke, A., Lyon, J. T., Haertelt, M., Meijer, G., Claes, P., De Haeck, J., and Lievens, P. (2009). Vibrational spectroscopy of neutral silicon clusters via far-IR-VUV two color ionization. *J. Chem. Phys.*, 131(17):171105.

Fitting, H., Ziems, T., von Czarnowski, A., and Schmidt, B. (2004). Luminescence center transformation in wet and dry SiO_2. *Radiat. Meas.*, 38(4–6):649–653.

Fowler, W., and Dexter, D. (1968). Electronic bubble states in liquid helium. *Phys. Rev.*, 176(1):337–343.

Fox, M. (2010). *Optical Properties of Solids*, vol. 3. Oxford University Press, Oxford, UK.

Fuke, K., Tsukamoto, K., Misaizu, F., and Sanekata, M. (1993). Near threshold photoionization of silicon clusters in the 248–146 nm region: Ionization potentials for Sin. *J. Chem. Phys.*, 99(10):7807–7812.

Galinis, G., Torricelli, G., Akraiam, A., and von Haeften, K. (2012a). Measurement of cluster-cluster interaction in liquids by deposition of silicon clusters onto HOPG surfaces. *J. Nanopart. Res.*, 14:1057.

Galinis, G., Yazdanfar, H., Bayliss, M., Watkins, M., and von Haeften, K. (2012b). Towards biosensing via fluorescent surface sites of nanoparticles. *J. Nanopart. Res.*, 14(8):1019.

Grass, M., Fischer, D., Mathes, M., Ganteför, G., and Nielaba, P. (2002). A form of bulk silicon consisting of "magic" clusters. *Appl. Phys. Lett.*, 81(20):3810–3812.

Grimes, C. C., and Adams, G. (1990). Infrared spectrum of the electron bubble in liquid helium. *Phys. Rev. B*, 41(10):6366–6371.

Grimes, C. C., and Adams, G. (1992). Infrared-absorption spectrum of the electron bubble in liquid helium. *Phys. Rev. B*, 45(5):2305.

Haberland, H., Karrais, M., and Mall, M. (1991). A new type of cluster and cluster ion source. *Z. Phys. D*, 20(1):413–415.

Halder, A., and Kresin, V. V. (2015). Nanocluster ionization energies and work function of aluminum, and their temperature dependence. *J. Chem. Phys.*, 143(16):164313.

Harbich, W., Sieber, C., Meiwes-Broer, K., and Félix, C. (2007). Electronic excitations induced by the impact of coinage metal ions and clusters on a rare gas matrix: Neutralization and luminescence. *Phys. Rev. B*, 76(10):104306.
Harris, C., Syväjärvi, M., Bergman, J., Kordina, O., Henry, A., Monemar, B., and Janzen, E. (1994). Time-resolved decay of the blue emission in porous silicon. *Appl. Phys. Lett.*, 65(19):2451–2453.
Hayes, W., and Stoneham, A. M. (2004). *Defects and Defect Processes in Nonmetallic Solids*. Dover, Mineloa, NY.
He, Y., Zhong, Y., Peng, F., Wei, X., Su, Y., Lu, Y., Su, S., Gu, W., Liao, L., and Lee, S.-T. (2011). One-pot microwave synthesis of water-dispersible, ultraphoto-and pH-stable, and highly fluorescent silicon quantum dots. *J. Angew. Chem. Int. Ed.*, 133(36):14192–14195.
Hirsch, K., Lau, J., Klar, P., Langenberg, A., Probst, J., Rittmann, J., Vogel, M., Zamudio-Bayer, V., Möller, T., and Issendorff, B. (2009). X-ray spectroscopy on size-selected clusters in an ion trap: From the molecular limit to bulk properties. *J. Phys. B*, 42:154029.
Hirschman, K., Tsybeskov, L., Duttagupta, S., and Fauchet, P. (1996). Silicon-based visible light-emitting devices integrated into microelectronic circuits. *Nature*, 384(6607):338–341.
Ho, K., Shvartsburg, A., Pan, B., Lu, Z., Wang, C., Wacker, J., Fye, J., and Jarrold, M. (1998). Structures of medium-sized silicon clusters. *Nature*, 392(6676):582–585.
Hoffmann, G., Kliewer, J., and Berndt, R. (2001a). Luminescence from metallic quantum wells in a scanning tunneling microscope. *Phys. Rev. Lett.*, 87(17):176803.
Hoffmann, M. A., Wrigge, G., Issendorff, B. V., Müller, J., Ganteför, G., and Haberland, H. (2001b). Ultraviolet photoelectron spectroscopy of Si 4- to Si 1000. *Eur. J. Phys. D Atmos. Mol. Clusters*, 16(1):9–11.
Hofmeister, H., Huisken, F., and Kohn, B. (1999). Lattice contraction in nanosized silicon particles produced by laser pyrolysis of silane. *Eur. J. Phys. D Atmos. Mol. Clusters Atomic Mol., Opt. Plasm. Phys.*, 9(1):137–140.
Honea, E. C., Kraus, J., Bower, J., and Jarrold, M. (1993a). Optical spectra of size-selected matrix-isolated silicon clusters. *Z. Phys. D Atmos. Mol. Clusters*, 26(1):141–143.
Honea, E. C., Ogura, A., Murray, C. A., Raghavachari, K., Sprenger, W. O., Jarrold, M. F., and Brown, W. L. (1993b). Raman spectra of size-selected silicon clusters and comparison with calculated structures. *Nature*, 366:40–44.
Honea, E.C, Ogura, A., Peale, D., Félix, C., Murray, C., Raghavachari, K., Sprenger, W., Jarrold, M., and Brown, W. (1999). Structures and coalescence behavior of size-selected silicon nanoclusters studied by surface-plasmon-polariton enhanced Raman spectroscopy. *J. Chem. Phys.*, 110:24.
Hoops, A. A., Bise, R.T., Choi, H., and Neumark, D. M. (2001). Photodissociation spectroscopy and dynamics of Si_4. *Chem. Phys. Lett.*, 346(1):89–96.
Hou, X., Shi, G., Wang, W., Zhang, F., Hao, P., Huang, D., and Wang, X. (1993). Large blue shift of light emitting porous silicon by boiling water treatment. *Appl. Phys. Lett.*, 62(10):1097–1098.
Hudgins, R. R., Imai, M., Jarrold, M. F., and Dugourd, P. (1999). High-resolution ion mobility measurements for silicon cluster anions and cations. *J. Chem. Phys.*, 111(17):7865–7870.
Huisken, F., Kohn, B., Alexandrescu, R., Cojocaru, S., Crunteanu, A., Ledoux, G., and Reynaud, C. (1999). Silicon carbide nanoparticles produced by CO2 laser pyrolysis of SiH_4/C_2H_2 gas mixtures in a flow reactor. *J. Nanopart. Res.*, 1(2):293–303.
Intartaglia, R., Bagga, K., Genovese, A., Athanassiou, A., Cingolani, R., Diaspro, A., and Brandi, F. (2012a). Influence of organic solvent on optical and structural properties of ultra-small silicon dots synthesized by UV laser ablation in liquid. *Phys. Chem. Chem. Phys.*, 14(44):15406–15411.
Intartaglia, R., Bagga, K., Scotto, M., Diaspro, A., and Brandi, F. (2012b). Luminescent silicon nanoparticles prepared by ultra short pulsed laser ablation in liquid for imaging applications. *Opt. Mat. Exp.*, 2(5):510–518.
Jackson, K. A., Horoi, M., Chaudhuri, I., Frauenheim, T., and Shvartsburg, A. A. (2004). Unraveling the shape transformation in silicon clusters. *Phys. Rev. Lett.*, 93(1):013401.
Jarrold, M. F., and Constant, V. A. (1991). Silicon cluster ions: Evidence for a structural transition. *Phys. Rev. Lett.*, 67(21):2994–2997.
Kanemitsu, Y., Futagi, T., Matsumoto, T., and Mimura, H. (1994). Origin of the blue and red photoluminescence from oxidized porous silicon. *Phys. Rev. B*, 49(20):14732–14735.
Kasigkeit, C., Hirsch, K., Langenberg, A., Moöller, T., Probst, J., Rittmann, J., Vogel, M., et al. (2015). Higher ionization energies from sequential vacuum-ultraviolet multiphoton ionization of size-selected silicon cluster cations. *J. Phys. Chem. C*, 119(20):11148–11152.
Katzy, R., Singer, M., Izadnia, S., LaForge, A., and Stienkemeier, F. (2016). Doping He droplets by laser ablation with a pulsed supersonic jet source. *Rev. Sci. Instrum.*, 87(1):013105.
Kimura, K. (1999). Blue luminescence from silicon nanoparticles suspended in organic liquids. *J. Cluster Sci.*, 10(2):359–380.
Kitsopoulos, T. N., Chick, C. J., Weaver, A., and Neumark, D. M. (1990). Vibrationally resolved photoelectron spectra of and. *J. Chem. Phys.*, 93(8):6108–6110.
Knight, W., Clemenger, K., de Heer, W., Saunders, W., Chou, M., and Cohen, M. (1984). Electronic shell structure and abundances of sodium clusters. *Phys. Rev. Lett.*, 52(24):2141–2143.

Kontkiewicz, A. J., Kontkiewicz, A. M., Siejka, J., Sen, S., Nowak, G., Hoff, A., Sakthivel, P., et al. (1994). Evidence that blue luminescence of oxidized porous silicon originates from SiO_{2n}. *Appl. Phys. Lett.*, 65(11):1436–1438.
Kovalev, D., Yaroshetzkii, I., Muschik, T., Petrova-Koch, V., and Koch, F. (1994). Fast and slow visible luminescence bands of oxidized porous Si. *Appl. Phys. Lett.*, 64(2):214–216.
Koyama, H., Matsushita, Y., and Koshida, N. (1998). Activation of blue emission from oxidized porous silicon by annealing in water vapor. *J. Appl. Phys.*, 83(3):1776–1778.
Kumar, V., and Kawazoe, Y. (2001). Metal-encapsulated fullerenelike and cubic caged clusters of silicon. *Phys. Rev. Lett.*, 87(4):045503.
Kumar, V., and Kawazoe, Y. (2003a). Hydrogenated silicon fullerenes: Effects of H on the stability of metal-encapsulated silicon clusters. *Phys. Rev. Lett.*, 90(5):055502.
Kumar, V., and Kawazoe, Y. (2003b). Metal-doped magic clusters of Si, Ge, and Sn: The finding of a magnetic superatom. *Appl. Phys. Lett.*, 83(13):2677–2679.
Laarmann, T., Wabnitz, H., von Haeften, K., and Möller, T. (2008). Photochemical processes in doped argon-neon core-shell clusters: The effect of cage size on the dissociation of molecular oxygen. *J. Chem. Phys.*, 128(1):014502.
Laguna, M., Paillard, V., Kohn, B., Ehbrecht, M., Huisken, F., Ledoux, G., Papoular, R., and Hofmeister, H. (1999). Optical properties of nanocrystalline silicon thin films produced by size-selected cluster beam deposition. *J. Lumin.*, 80(1–4):223–228.
Lau, J., Vogel, M., Langenberg, A., Hirsch, K., Rittmann, J., Zamudio-Bayer, V., Möller, T., and von Issendorff, B. (2011). Communication: Highest occupied molecular orbital–lowest unoccupied molecular orbital gaps of doped silicon clusters from core level spectroscopy. *J. Chem. Phys.*, 134(4):041102.
Ledoux, G., Amans, D., Gong, J., Huisken, F., Cichos, F., and Martin, J. (2002). Nanostructured films composed of silicon nanocrystals. *Mater. Sci. Eng. C*, 19(1–2):215–218.
Ledoux, G., Gong, J., and Huisken, F. (2001). Effect of passivation and aging on the photoluminescence of silicon nanocrystals. *Appl. Phys. Lett.*, 79(24):4028–4030.
Ledoux, G., Guillois, O., Porterat, D., Reynaud, C., Huisken, F., Kohn, B., and Paillard, V. (2000). Photoluminescence properties of silicon nanocrystals as a function of their size. *Phys. Rev. B*, 62(23):15942–15951.
Li, Q., He, Y., Chang, J., Wang, L., Chen, H., Tan, Y.-W., Wang, H., and Shao, Z. (2013). Surface-modified silicon nanoparticles with ultrabright photoluminescence and single-exponential decay for nanoscale fluorescence lifetime imaging of temperature. *J. Am. Chem. Soc.*, 135(40):14924–14927.
Li, Q., Luo, T.-Y., Zhou, M., Abroshan, H., Huang, J., Kim, H. J., Rosi, N. L., Shao, Z., and Jin, R. (2016). Silicon nanoparticles with surface nitrogen: 90% quantum yield with narrow luminescence bandwidth and the ligand structure based energy law. *ACS Nano*, 10(9):8385–8393.
Li, X., He, Y., and Swihart, M. T. (2004a). Surface functionalization of silicon nanoparticles produced by laser-driven pyrolysis of silane followed by HF-HNO_3 etching. *Langmuir*, 20(11):4720–4727.
Li, X., He, Y., Talukdar, S., and Swihart, M. (2004b). Preparation of luminescent silicon nanoparticles by photothermal aerosol synthesis followed by acid etching. *Phase Transitions*, 77(1–2):131–137.
Li, Z., and Ruckenstein, E. (2004). Water-soluble poly (acrylic acid) grafted luminescent silicon nanoparticles and their use as fluorescent biological staining labels. *Nano Lett.*, 4(8):1463–1467.
Lockwood, D. (1994). Optical properties of porous silicon. *Solid State Commun.*, 92(1–2):101–112.
Lockwood, D. J., Lu, Z. H., and Baribeau, J.-M. (1996). Quantum confined luminescence in Si/SiO_2 superlattices. *Phys. Rev. Lett.*, 76(3):539.
Loni, A., Simons, A., Calcott, P., and Canham, L. (1995). Blue photoluminescence from rapid thermally oxidized porous silicon following storage in ambient air. *J. Appl. Phys.*, 77(7):3557–3559.
Lyon, J. T., Gruene, P., Fielicke, A., Meijer, G., Janssens, E., Claes, P., and Lievens, P. (2009). Structures of silicon cluster cations in the gas phase. *J. Angew. Chem. Int. Ed.*, 131(3):1115–1121.
Mangolini, L., Thimsen, E., and Kortshagen, U. (2005). High-yield plasma synthesis of luminescent silicon nanocrystals. *Nano Lett.*, 5(4):655–659.
Marsen, B., Lonfat, M., Scheier, P., and Sattler, K. (2000). Energy gap of silicon clusters studied by scanning tunneling spectroscopy. *Phys. Rev. B*, 62(11):6892–6895.
Maus, M., Ganteför, G., and Eberhardt, W. (2000). The electronic structure and the band gap of nano-sized Si particles: Competition between quantum confinement and surface reconstruction. *Appl. Phys. A Mater. Sci. Process.*, 70(5):535–539.
McVey, B. F., and Tilley, R. D. (2014). Solution synthesis, optical properties, and bioimaging applications of silicon nanocrystals. *Acc. Chem. Res.*, 47(10):3045–3051.
Meloni, G., Ferguson, M. J., Sheehan, S. M., and Neumark, D. M. (2004). Probing structural transitions of nanosize silicon clusters via anion photoelectron spectroscopy at 7.9 eV. *Chem. Phys. Lett.*, 399(4):389–391.
Mitas, L., Grossman, J. C., Stich, I., and Tobik, J. (2000). Silicon clusters of intermediate size: Energetics, dynamics, and thermal effects. *Phys. Rev. Lett.*, 84(7):1479–1482.

Montalti, M., Cantelli, A., and Battistelli, G. (2015). Nanodiamonds and silicon quantum dots: Ultrastable and biocompatible luminescent nanoprobes for long-term bioimaging. *Chem. Soc. Rev.*, 44(14):4853–4921.

Nel, A., Madler, L., Velegol, D., Xia, T., Hoek, E., Somasundaran, P., Klaessig, F., Castranova, V., and Thompson, M. (2009). Understanding biophysicochemical interactions at the nano-bio interface. *Nat. Mater.*, 8(7):543–557.

Nishikawa, H., Shiroyama, T., Nakamura, R., Ohki, Y., Nagasawa, K., and Hama, Y. (1992). Photoluminescence from defect centers in high-purity silica glasses observed under 7.9-eV excitation. *Phys. Rev. B*, 45(2):586–591.

Ondič, L., Kusová, K., Ziegler, M., Fekete, L., Gärtnerová, V., Cháb, V., Holỳ, V., et al. (2014). A complex study of the fast blue luminescence of oxidized silicon nanocrystals: The role of the core. *Nanoscale*, 6(7):3837–3845.

Park, J., Gu, L., von Maltzahn, G., Ruoslahti, E., Bhatia, S., and Sailor, M. (2009). Biodegradable luminescent porous silicon nanoparticles for in vivo applications. *Nat. Mater.*, 8(4):331–336.

Park, N., Kim, T., and Park, S. (2001). Band gap engineering of amorphous silicon quantum dots for light-emitting diodes. *Appl. Phys. Lett.*, 78:2575.

Pavesi, L. (2003). Will silicon be the photonic material of the third millenium? *J. Phys. C*, 15:1169.

Pavesi, L., Negro, L. D., Mazzoleni, C., Franzò, G., and Priolo, F. (2000). Optical gain in silicon nanocrystals. *Nature*, 408:440–444.

Peng, F., Su, Y., Zhong, Y., Fan, C., Lee, S.-T., and He, Y. (2014). Silicon nanomaterials platform for bioimaging, biosensing, and cancer therapy. *Acc. Chem. Res.*, 47(2):612–623.

Pratontep, S., Carroll, S. J., Xirouchaki, C., Streun, M., and Palmer, R. E. (2005). Size-selected cluster beam source based on radio frequency magnetron plasma sputtering and gas condensation. *Rev. Sci. Instrum.*, 76:045103.

Priolo, F., Gregorkiewicz, T., Galli, M., and Krauss, T. F. (2014). Silicon nanostructures for photonics and photovoltaics. *Nat. Nanotechnol.*, 9(1):19–32.

Raghavachari, K. (1986). Theoretical study of small silicon clusters: Equilibrium geometries and electronic structures of Si_n (n= 2–7, 10). *J. Chem. Phys.*, 84(10):5672–5686.

Raghavachari, K., and Logovinsky, V. (1985). Structure and bonding in small silicon clusters. *Phys. Rev. Lett.*, 55(26):2853.

Raghavachari, K., and Rohlfing, C. M. (1988). Bonding and stabilities of small silicon clusters: A theoretical study of Si_7 Si_{10}. *J. Chem. Phys.*, 89(4):2219–2234.

Rodio, M., Brescia, R., Diaspro, A., and Intartaglia, R. (2016). Direct surface modification of ligand-free silicon quantum dots prepared by femtosecond laser ablation in deionized water. *J. Colloid Interface Sci.*, 465:242–248.

Sattler, K., Mühlbach, J., and Recknagel, E. (1980). Generation of metal clusters containing from 2 to 500 atoms. *Phys. Rev. Lett.*, 45(10):821–824.

Seraphin, A., Ngiam, S.-T., and Kolenbrander, K. (1996). Surface control of luminescence in silicon nanoparticles. *J. Appl. Phys.*, 80(11):6429–6433.

Sieber, C., Buttet, J., Harbich, W., Felix, C., Mitric, R., and Bonacic-Koutecky, V. (2004). Isomer-specific spectroscopy of metal clusters trapped in a matrix: Ag_9. *Phys. Rev. A*, 70(4):041201.

Skuja, L. (1992). Isoelectronic series of twofold coordinated Si, Ge, and Sn atoms in glassy SiO_2: A luminescence study. *J. Non-Cryst. Solids*, 149(1/2):77–95.

Skuja, L., Streletsky, A., and Pakovich, A. (1984). A new intrinsic defect in amorphous SiO_2: Twofold coordinated silicon. *Solid State Commun.*, 50(12):1069–1072.

Stupca, M., Alsalhi, M., Al Saud, T., Almuhanna, A., and Nayfeh, M. (2007). Enhancement of polycrystalline silicon solar cells using ultrathin films of silicon nanoparticle. *Appl. Phys. Lett.*, 91:063107.

Sun, Q., Wang, Q., Jena, P., Rao, B. K., and Kawazoe, Y. (2003). Stabilization of SiO_{60} cage structure. *J Phys. Rev. Lett.*, 90(13):135503.

Švrček, V., Mariotti, D., Cvelbar, U., Filipič, G., Lozach, M., McDonald, C., Tayagaki, T., and Matsubara, K. (2016). Environmentally friendly processing technology for engineering silicon nanocrystals in water with laser pulses. *J. Phys. Chem. C*, 120(33):18822–18830.

Švrček,, V., Mariotti, D., and Kondo, M. (2009a). Ambient-stable blue luminescent silicon nanocrystals prepared by nanosecond-pulsed laser ablation in water. *Opt. Express.*, 17(2):520–527.

Švrček, V., Sasaki, T., Katoh, R., Shimizu, Y., and Koshizaki, N. (2009b). Aging effect on blue luminescent silicon nanocrystals prepared byápulsed laser ablation of silicon wafer in de-ionized water. *Appl. Phys. B*, 94(1):133–139.

Švrček, V., Slaoui, A., and Muller, J. (2004). Silicon nanocrystals as light converter for solar cells. *Thin Solid Films*, 451:384–388.

Takagi, H., Ogawa, H., Yamazaki, Y., Ishizaki, A., and Nakagiri, T. (1990). Quantum size effects on photoluminescence in ultrafine Si particles. *Appl. Phys. Lett.*, 56:2379.

Tománek, D., and Schlüter, M. (1986). Calculation of magic numbers and the stability of small Si clusters. *Phys. Rev. Lett.*, 56(10):1055–1058.

Torricelli, G., Akraiam, A., and von Haeften, K. (2011). Size-selecting effect of water on fluorescent silicon clusters. *Nanotechnology*, 22:315711.

Tsybeskov, L., Vandyshev, J. V., and Fauchet, P. (1994). Blue emission in porous silicon: Oxygen-related photoluminescence. *Phys. Rev. B*, 49(11):7821.

Valenta, J., Fucikova, A., Pelant, I., Kusová, K., Dohnalová, K., Aleknavičius, A., Cibulka, O., Fojtík, A., and Kada, G. (2008). On the origin of the fast photoluminescence band in small silicon nanoparticles. *New J. Phys.*, 10:073022.

Vincent, J., Maurice, V., Paquez, X., Sublemontier, O., Leconte, Y., Guillois, O., Reynaud, C., Herlin-Boime, N., Raccurt, O., and Tardif, F. (2010). Effect of water and UV passivation on the luminescence of suspensions of silicon quantum dots. *J. Nanopart. Res.*, 12(1):39–46.

Vogel, M., Kasigkeit, C., Hirsch, K., Langenberg, A., Rittmann, J., Zamudio-Bayer, V., Kulesza, A., et al. (2012). 2p core-level binding energies of size-selected free silicon clusters: Chemical shifts and cluster structure. *Phys. Rev. B*, 85(19):195454.

von Haeften, K., Akraiam, A., Torricelli, G., and Brewer, A. (2010a). Fluorescence of silicon nanoparticles suspended in water: Reactive co-deposition for the control of surface properties of clusters. *AIP Conf. Proc.*, 1275:40.

von Haeften, K., Binns, C., Brewer, A., Crisan, O., Howes, P., Lowe, M., Sibbley-Allen, C., and Thornton, S. C. (2009). A novel approach towards the production of luminescent silicon nanoparticles: Sputtering, gas aggregation and co-deposition with H_2O. *Eur. Phys. J. D*, 52(1–3):11–14.

von Haeften, K., Lowe, M., and Brewer, A. (2010b). *Fluorescence of Silicon Nanoparticles Suspended in Water*. Innsbruck University Press, Innsbruck, Austria.

Warner, J., Hoshino, A., Yamamoto, K., and Tilley, R. (2005). Water-soluble photoluminescent silicon quantum dots. *Angew. Chem. Int. Ed.*, 44(29):4550–4553.

Wegner, K., Piseri, P., Tafreshi, H., and Milani, P. (2006). Cluster beam deposition: A tool for nanoscale science and technology. *J. Phys. D Appl. Phys.*, 39(22):R439–R459.

Wilson, W., Szajowski, P., and Brus, L. (1993). Quantum confinement in size-selected, surface-oxidized silicon nanocrystals. *Science*, 262(5137):1242–1244.

Xu, C., Taylor, T. R., Burton, G. R., and Neumark, D. M. (1998). Vibrationally resolved photoelectron spectroscopy of silicon cluster anions Si − n(n = 3–7). *J. Chem. Phys.*, 108(4):1395–1406.

Yamani, Z., Thompson, W. H., AbuHassan, L., and Nayfeh, M. H. (1997). Ideal anodization of silicon. *Appl. Phys. Lett.*, 70(25):3404–3406.

Yazdanfar, H., Kotlov, A., and von Haeften, K. (2012). *Blue Photoluminescence of Oxidised Silicon Nanoparticles in Solution and on Surfaces.* Technical report. DESY Photon Science, Annual Report, Hamburg, Germany.

Yu, D., Hang, Q., Ding, Y., Zhang, H., Bai, Z., Wang, J., Zou, Y., Qian, W., Xiong, G., and Feng, S. (1998). Amorphous silica nanowires: Intensive blue light emitters. *Appl. Phys. Lett.*, 73:3076.

Zhong, Y., Peng, F., Bao, F., Wang, S., Ji, X., Yang, L., Su, Y., Lee, S.-T., and He, Y. (2013). Large-scale aqueous synthesis of fluorescent and biocompatible silicon nanoparticles and their use as highly photostable biological probes. *J. Am. Chem. Soc.*, 135(22):8350–8356.

Žídek, K., Trojanek, F., Malỳ, P., Pelant, I., Gilliot, P., and Hönerlage, B. (2011). Ultrafast photoluminescence dynamics of blue-emitting silicon nanostructures. *Phys. Stat. Sol. (c)*, 8(3):979–984.